Dynamic Feedforward Control for an Active Three Phase EMI Filter

M. Sc. Stefan Haensel, Siemens AG, Germany
Dipl.-Ing. Sebastian Nielebock, Siemens AG, Germany
Prof. Dr.-Ing. Stephan Frei, TU Dortmund, Germany

1 Introduction

Power electronic systems usually produce high amounts of electromagnetic interferences (EMI) due to PWM operation. To comply with international standards on electromagnetic compatibility (EMC), e. g. EN 61800-3 in industrial applications [1], the EMI shall not exceed given limits. To reach these limits often filters need to be integrated into the system. The common solution is to add passive EMI filters consisting of capacitors and inductors [2]. Passive filters are often bulky and heavy, therefore active cancellation techniques for power electronic systems were introduced [3]. Active EMI filter (AEF) consists of an analog (and rarely also digital) circuit to actively suppress the disturbances by injecting an anti-noise signal.
As discussed in [4], well-known closed loop feedforward or feedback structures for AEF have their limitation specially because of the limited amplifiers open-loop gain, delays due to the finite signal propagation speed in the circuit and the measurement accuracy. For this reason, active EMI cancellation by injecting synthesized signals was introduced.
This paper introduces a method for generating a synthesized signal for a three-phase grid converter.

2 Mathematic description of an AEF connected to a three-phase grid converter

AEF for three phase converters were already introduced in [5, 6], but they focused on the active cancellation of common mode noise. But in many cases cancellation of common mode and differential mode noise is required. In [5] the anti-noise signal is coupled capacitively into the noisy circuit, in [6] it is inductively coupled. Both circuits can be adapted to cancel common and differential mode noise, but for simplification reasons only the capacitive coupled system will be discussed in detail. In Figure 1, the basic system setup for an active cancellation of common and differential mode noise is shown. It consists of a three phase grid, a line impedance stabilization network (LISN), a common mode inductor, a capacitive coupled AEF, a coupled boost inductance and a converter.

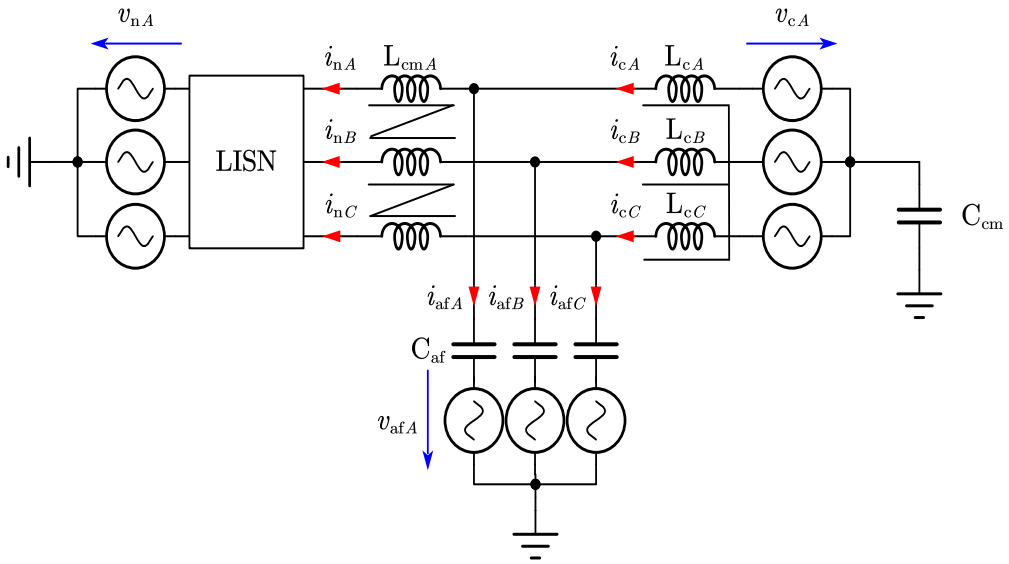

Figure 1: Equivalent circuit of the converter with anti-noise source
Grid voltage, LISN, common-mode inductor, AEF capacitively coupled, converter with boost choke

CISPR-16-1-2 allows several implementations for the LISN. An implementation, which fulfils specification for frequency band A and B is shown in Figure 2 on the left side. Low frequency components of the current can pass the LISN, so that power can be transferred, high frequency components get blocked and can be measured as v_{emi}. It is assumed, an AEF should only suppress the frequency bands A and B. In this case the system can be simplified so that lower frequencies can be ignored. All further equations are valid for frequencies above 9 kHz. For frequencies above 9 kHz the LISN can be simplified as shown in Figure 2 on right side, which shows the decoupling of the grid.
For a first investigation it will be assumed that impedances in all three phases are equal so that an extended Clarke transformation [7] can be used to separate the three phases into an α, β and 0 system, which is shown in Figure 3.

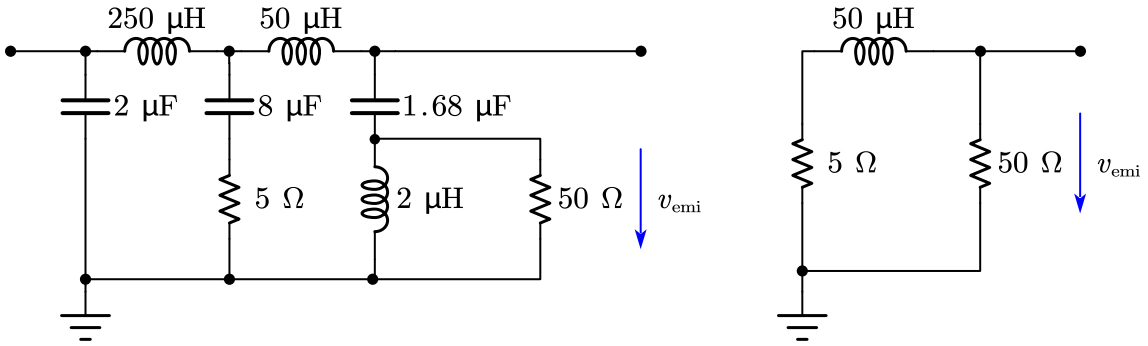

Figure 2: Line impedance stabilization network (LISN)
left: Full frequency representation, right: simplified representation for frequencies above 9 kHz

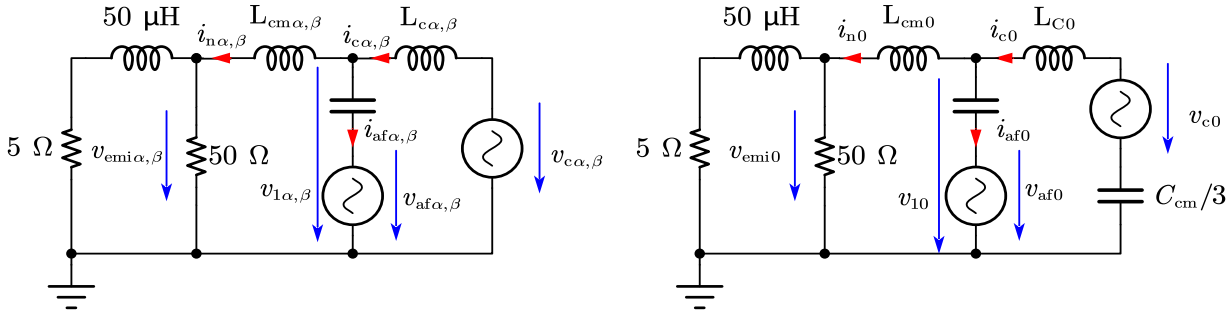

Figure 3: Equivalent circuit of the converter and the AEF in α, β and 0 system

(1) to (3) show that the 0-components of the Clarke transformation represent the common mode and the α and β-components represent differential mode.

$$V_{\mathrm{cm}} = \frac{1}{3}(V_a + V_b + V_c) = \sqrt{3}\sqrt{\frac{2}{3}}\left(\frac{1}{\sqrt{2}}V_a + \frac{1}{\sqrt{2}}V_b + \frac{1}{\sqrt{2}}V_b\right) = \sqrt{3}V_0 \tag{1}$$

$$V_{dmcb} = V_c - V_b = \sqrt{2}\sqrt{\frac{2}{3}}\left(\frac{\sqrt{3}}{2}V_b - \frac{\sqrt{3}}{2}V_c\right) = \sqrt{2}V_\beta \tag{2}$$

$$V_{\mathrm{dm}ab} = V_a - V_b = \sqrt{\frac{2}{3}}\left(V_a - \frac{1}{2}V_b - \frac{1}{2}V_c\right) - \frac{1}{\sqrt{3}}\sqrt{\frac{2}{3}}\left(\frac{\sqrt{3}}{2}V_b + \frac{\sqrt{3}}{2}V_c\right) = \sqrt{\frac{3}{2}}\left(V_\alpha - \frac{1}{\sqrt{3}}V_\beta\right) \tag{3}$$

The behavior of the system can now be described in Laplace domain.
Assuming the converter voltage v_c is the disturbance in the system, which generates an additional noise current in the grid i_n, a voltage v_{af} needs to be found that cancels these disturbances. For that the voltage v_1 needs to be zero for all complex frequencies s.

$$V_{1\alpha,\beta} = V_{\mathrm{af}\alpha,\beta} + I_{\mathrm{af}\alpha,\beta} \cdot Z_{C\mathrm{af}} = V_{\mathrm{c}\alpha,\beta} - I_{\mathrm{c}\alpha,\beta} \cdot Z_{Lc} = 0 \tag{4}$$

$$V_{\mathrm{af}\alpha,\beta} = \frac{Z_{C\mathrm{af}\alpha,\beta}}{Z_{Lc\alpha,\beta}} \cdot V_{c\alpha,\beta} = \frac{1}{L_{\mathrm{c}} C_{\mathrm{af}} s^2} \cdot V_{\mathrm{c}\alpha,\beta} \tag{5}$$

And similar for the 0-system

$$V_{\mathrm{af0}} = \frac{Z_{C\mathrm{af}}}{(Z_{Lc0} + Z_{C\mathrm{cm}})} \cdot V_{\mathrm{c0}} = \frac{1}{C_{\mathrm{af}} \cdot \left(L_c s^2 + \frac{3}{C_{\mathrm{cm}}}\right)} \cdot V_{\mathrm{c0}} \tag{6}$$

These correlations describe a dynamic feedforward control for an AEF for a three-phase system.

3 Limitations of feed forward control

The feedforward control described by (5) and (6) will cancel out all disturbances introduced by the converter if the mathematic description of the whole system is accurate. But parameters of most components are frequency dependent and variation in parameters and coupling between phases can introduce asymmetry. While a frequency dependency can be modeled easily into the introduced feed forward control by using transfer functions for the impedances $Z_{C\mathrm{af}}$, Z_{Lc} and $Z_{C\mathrm{cm}}$, an asymmetry will cause off-diagonal elements in Clarke's transfer matrix $\boldsymbol{T}$ to not equal zero, so that a coupling between α, β and 0 system is still there. This coupling prohibits a strict separation between common mode and differential mode noise because a common mode disturbance v_{c0} will not only result in a common mode noise v_{emi0}, but also in a differential mode noise $v_{\mathrm{emi}\alpha,\beta}$.
To investigate the effect of asymmetric components on the feedforward control, a simulation according to Figure 4 with parameters shown in Table 1 is setup in MATLAB Simulink.

Table 1: Parameter for simulation

Parameter	Value
V_{DC}	800 V
L_{C}	800 µH
L_{cm}	700 µH
C_{af}	1 µF
C_{cm}	1 nF
$f_{\mathrm{switching}}$	10 kHz

To evaluate effectiveness of the feed forward control, the simulation is run with AEF deactivated and activated. To compare the remaining disturbances v_{emi} with the allowed limits of EN 61800, an implementation of a CISPR detectors is needed. In [8], an implementation is introduced that is used for this comparison. The results of band A and band B disturbances of phase A are shown in Figure 5. Since phase A, B and C are symmetric, the disturbances are equal in all phases.
In simulation a reduction of more than 80 dB over the whole frequency range is possible with a symmetric setup.
To understand the impact of asymmetrical components, several simulations are conducted, with slightly different values for the converter inductance in phase A L_{cA} and the minimal reduction is calculated for each test point.
For further investigation, the asymmetry is defined as:

$$L_{cA} = L_{\mathrm{csym}} \cdot (1 + k) \qquad k = [0 \ldots 10]\ \% \tag{7}$$

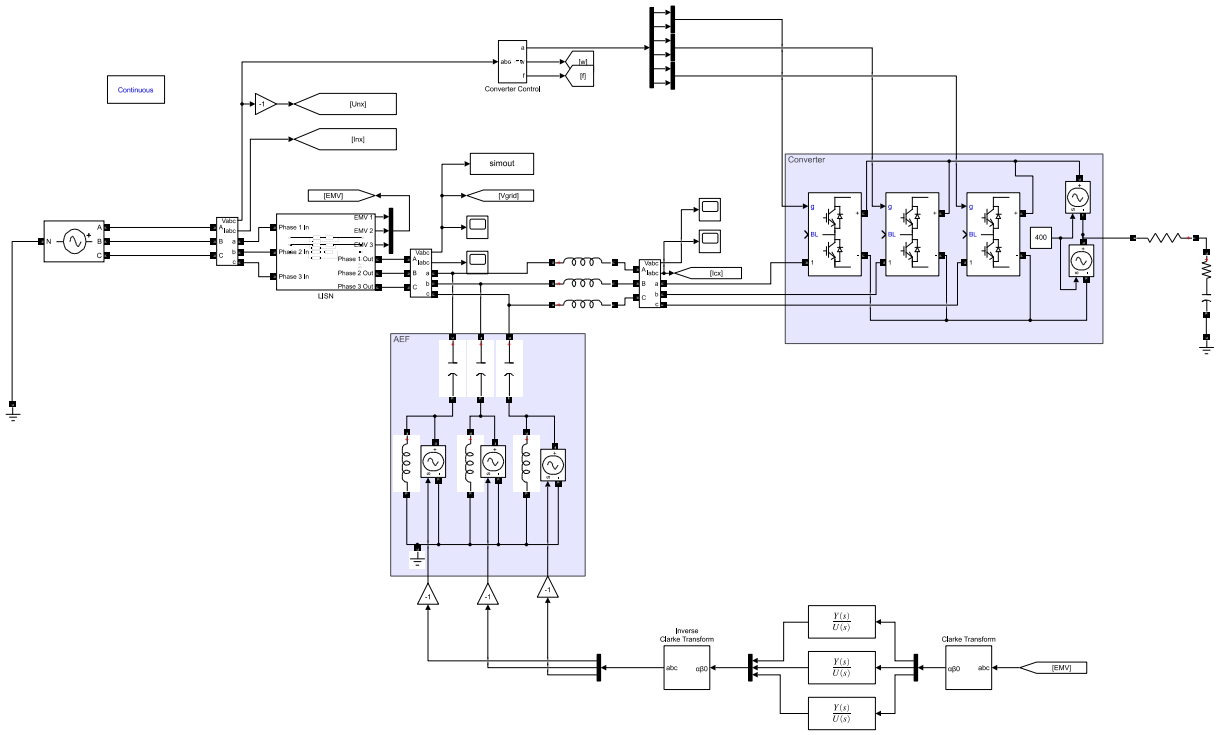

Figure 4: Simulation of a three-phase grid converter with feedforward control of an AEF

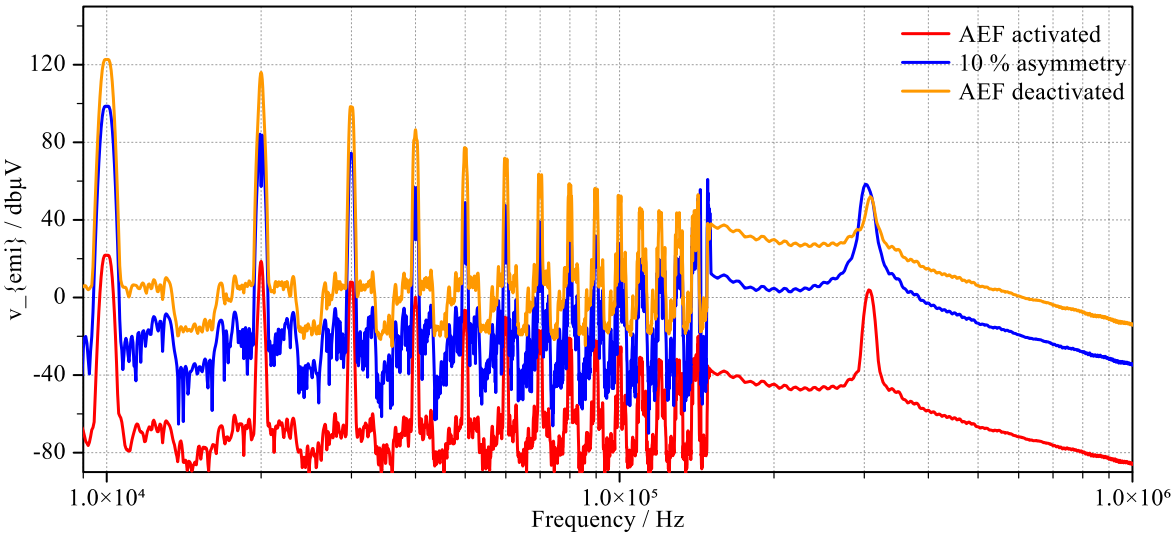

Figure 5: Disturbance with deactivated AEF and activated AEF

In Table 2, the remaining noise v_{emi} is listed at 10 kHz and 200 kHz with different asymmetries. It can be seen, that with rising asymmetry the remaining noise increases from 21.7 dBµV at ideal symmetry to 98.6 dBµV at 10% asymmetry.

Table 2: Remaining maximum noise v_{emi}

Setup	v_{emi} @10 kHz / dBµV	v_{emi} @200 kHz / dBµV
symmetric	21.7 (12 µV)	-44.7 (5.82 nV)
0.5% asymmetry	74.5 (5.3 mV)	-20 (0.097 µV)
1 % asymmetry	79.5 (9.5 mV)	-15 (0.184 µV)
2 % asymmetry	85.2 (18.2 mV)	-8.8 (0.361 µV)
4 % asymmetry	91.0 (35.7 mV)	-2.9 (0.713 µV)
6 % asymmetry	94.4 (52.8 mV)	0.50 (1.06 µV)
8 % asymmetry	96.8 (69 .5mV)	2.92 (1.40 µV)
10 % asymmetry	98.6 (85.7 mV)	4.79 (1.74 µV)
AEF disabled	122.7 (1.37 V)	29.8 (31.2 µV)

4 Measurement results

A setup with a 16 kW converter connected to a three phase LISN is built up for validation. For the test the AEF voltages v_{af} and the converter disturbance voltage v_{c} are implemented by six amplifiers of the type ADA4870ARR-EBZ, which are connected to an arbitrary waveform generator 33220A from Keysight and the remaining disturbances are measured by an EMI test receiver ESCI 7 from Rohde & Schwarz. The setup is shown in Figure 6.

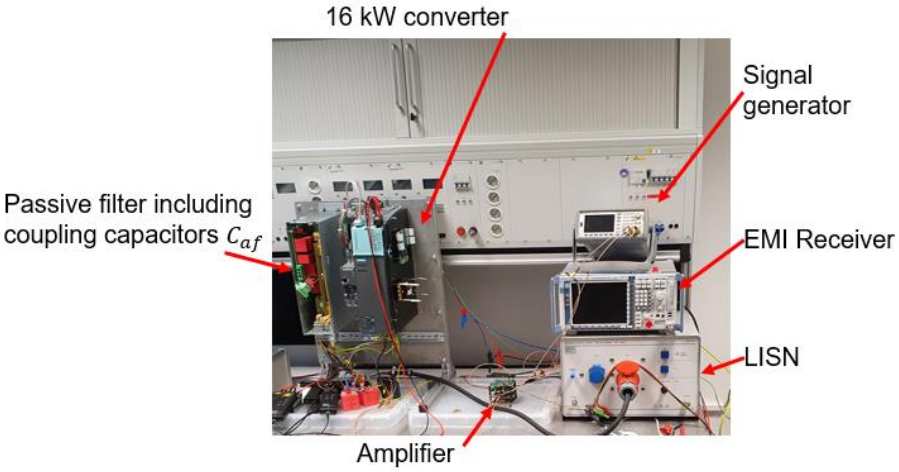

Figure 6: Laboratory setup of a 16 kW grid converter with capacitive coupled amplifiers

For identification of the coupled inductor L_{c}, a Bode100 from Omicron is used and measured as described in [9, S. 394]. The result for phase A, plotted in Figure 7, shows a decrease of the self-inductance L11 over the frequency, and a slight increase of the mutual-inductance M12 until 1 MHz. From 1 MHz on, the parasitic capacitance becomes dominant and the measured inductance becomes negative.

Table 3: Inductivity of converter inductance L_c for all three phases

	@1 kHz / µH	**@200 kHz / µH**
L11	648	418
L22	633	438
L33	646	424
M12	119	114
M13	105	65.7
M23	117	105

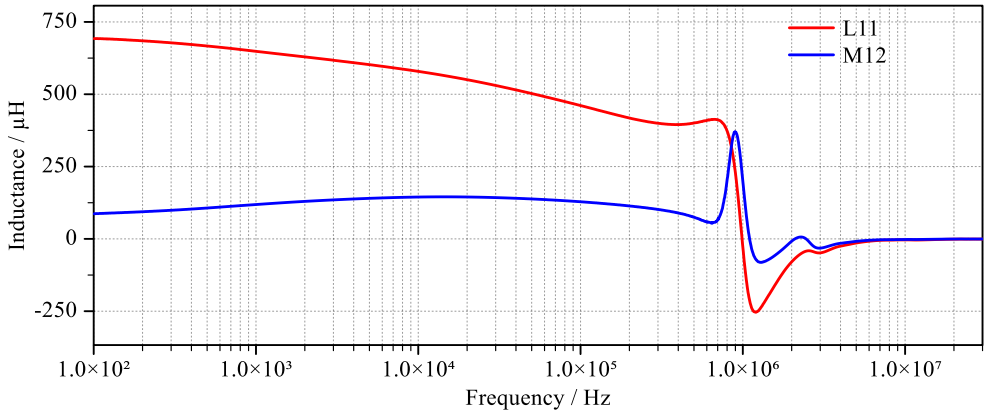

Figure 7: Self and mutual inductance of the converter inductor L_c

In Table 3 the inductance of all three phases at 1 kHz and 200 kHz are listed and a difference at 1 kHz for the self-inductances L_{xx} of 2.3% and for the mutual inductances M_{xy} of 11.8% can be seen. By using (9) and (10), the asymmetry of β-System and 0-system can be calculated to 3.6% and 0.8%, which will reduce the achievable EMI-reduction in the simulation by more than 40 dB.

$$L_\alpha = L_{xx} - \frac{1}{2}\left(M_{xy} + M_{xz}\right) \tag{8}$$

$$L_\beta = L_{xx} - M_{xy} \tag{9}$$

$$L_0 = L_{xx} + M_{xy} + M_{xz} \tag{10}$$

For verification a variable frequency sinusoidal waveform with 10 V amplitude is generated, which is used as converter voltage. For the active filter voltage, a sinusoidal waveform with the same frequency is used and phase and amplitude are adjusted, so that the remaining disturbance in phase B $v_{\mathrm{emi}B}$ reaches its minimum. In the next step the remaining disturbances in phase A and C are measured.
In the first setup only the β-system is stimulated by choosing $v_{\mathrm{c}A} = 0\,\mathrm{V}$, $v_{\mathrm{c}B} = 10\,\mathrm{V}$ and $v_{\mathrm{c}C} = -10\,\mathrm{V}$. In Figure 8 the strong performance for phase B of more than 30 dB reduction over the whole frequency range can be noticed. For phase C a strong performance at 10 kHz of 53.8 dB can be seen, which is 9.5 dB less than for phase B. With rising frequency, the performance for phase C decreases rapidly. At 50 kHz, there is no damping anymore. Although there is no noise directly injected into phase A, a high value of 92 dBµV is measured at 150 kHz. This is an indicator that a strong asymmetric coupling between the phases is present and since the coupling increases with rising frequency it can be assumed, that it is a capacitive coupling.
In the next setup all converter voltages v_{cABC} are equal to 10 V, so that the 0-system is analyzed. In Figure 9 a reduction of the disturbance of more than 50 dB can be seen at low frequencies for phase B and minimal 18.7 dB at 500 kHz. But for phase A and C only a very low reduction of 14.0 dB can be noticed. At 50 kHz, even an increase of noise in phase A can be seen.

For the common mode and the differential mode performance, it can be noticed that the performance over the whole frequency range was good for only the phase for which the signal was tuned. This can have several causes. For low frequencies till 50 kHz, the asymmetry of the inductor may be the main reason why the differential mode performance in phase C is reduced by 9.5 dB. But for higher frequencies and for the common mode performance, there may be several other effects. One effect may be the parameter variations of the analog amplifiers, which may result in errors in common mode voltage v_{c0} and v_{af0} and therefore a limited performance. Also, the parasitic capacitive coupling between phases and phases-to-ground may play an important role. Possibly the most important factor is the geometry of the inductor itself, so that the routing of the wiring is not perfectly symmetrical.

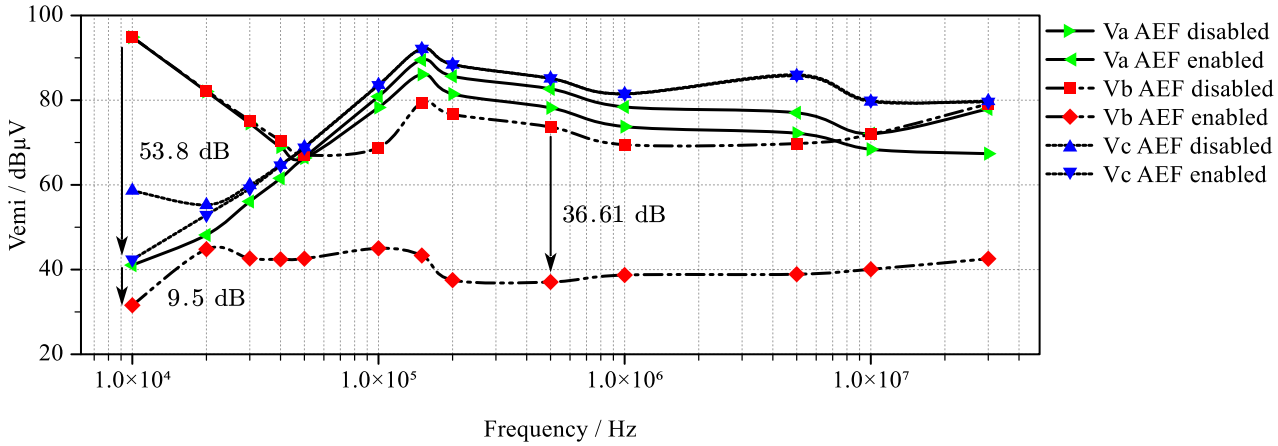

Figure 8: AEF performance for dm disturbance

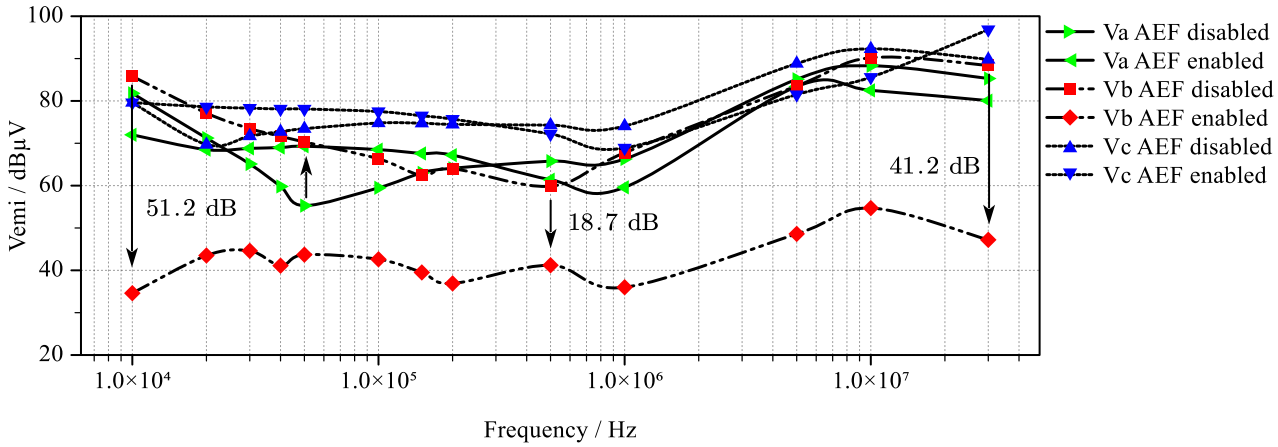

Figure 9: AEF performance for cm disturbance

It can be summarized that a feed forward control shows strong performance in simulation and also in single phases, but due to the Clarke transformation, which separates common and differential mode into separate circuit diagrams by assuming symmetrical components, a limited performance can be achieved in a laboratory setup.

3 Conclusion

In this paper, a dynamic feedforward control for the generation of synthesized signals to cancel EMI in a three-phase grid converter is discussed. With a Clarke transformation, two second order transfer functions can be derived, with which the control signals for an AEF can be synthetized. The effectiveness and limitations due to asymmetries are shown in simulation and measurement. In measurements, a strong suppression of differential EMI by more than 30 dB in the range of 9 kHz till 30 MHz is possible. But the assumption of symmetry of Clarke's transformation limits the performance of this feedforward control. It can be concluded that a strict separation of common mode and differential mode damping is not suited for active EMI filters. To improve the performance of this method, a full representation including off-diagonal elements will be considered in future, but it will increase the characterization and calculation effort.

References

Literatur

[1] *Adjustable speed electrical power drive systems - Part3: EMC requirements and specific test methods*, 61800-3, VDE, 2017.

[2] K. Mainali und R. Oruganti, „Conducted EMI Mitigation Techniques for Switch-Mode Power Converters: A Survey“, *IEEE Trans. Power Electron.*, Jg. 25, Nr. 9, S. 2344–2356, 2010, doi: 10.1109/TPEL.2010.2047734.

[3] S. Feng, W. Sander und T. Wilson, „Small-capacitance nondissipative ripple filters for DC supplies“, *IEEE Trans. Magn.*, Jg. 6, Nr. 1, S. 137–142, 1970, doi: 10.1109/TMAG.1970.1066675.

[4] A. Bendicks, T. Dorlemann, T. Osterburg und S. Frei, „Active cancellation of periodic EMI of power electronic systems by injecting artificially synthesized signals“, *IEEE Electromagn. Compat. Mag.*, Jg. 9, Nr. 3, S. 63–72, 2020, doi: 10.1109/MEMC.2020.9241554.

[5] S. Ogasawara, H. Ayano und H. Akagi, „An active circuit for cancellation of common-mode voltage generated by a PWM inverter“, *IEEE Trans. Power Electron.*, Jg. 13, Nr. 5, S. 835–841, 1998, doi: 10.1109/63.712285.

[6] I. Takahashi, „Active EMI Filter for Switching Noise of High Frequency Inverters“, *Proceedings of Power Conversion Conference - PCC '97*, 1997, doi: 10.1109/PCCON.1997.645634.

[7] E. H. Watanabe, R. M. Stephan und M. Aredes, „New concepts of instantaneous active and reactive powers in electrical systems with generic loads“, *IEEE Trans. Power Delivery*, Jg. 8, Nr. 2, S. 697–703, 1993, doi: 10.1109/61.216877.

[8] K. Hormaier, H. Zangl und H. Zojer, „An EMI receiver model to evaluate electromagnetic emissions by simulation“ in *2012 IEEE International Instrumentation and Measurement Technology Conference (I2MTC)*, Graz, Austria, 2012, S. 2558–2562, doi: 10.1109/I2MTC.2012.6229516.

[9] A. van den Bossche, *"Inductors and transformers for power electronics"*. Boca Raton, Fla. [u.a.]: Taylor & Francis, 2005.